Theoretical and computational studies of excitons in conjugated polymers

William Barford,[1,*] Robert J. Bursill,[2] and Richard W. Smith[1]

[1]*Department of Physics and Astronomy, The University of Sheffield, Sheffield, S3 7RH, United Kingdom*
[2]*School of Physics and Astronomy, The University of New South Wales, Sydney, NSW 2052, Australia*

We present a theoretical and computational analysis of excitons in conjugated polymers. We use a tight-binding model of π-conjugated electrons, with $1/r$ interactions for large r. In both the weak-coupling limit (defined by $W \gg U$) and the strong-coupling limit (defined by $W \ll U$), where W is the bandwidth and U is the on-site Coulomb interaction, we derive and analyze effective-particle models. We compare these to density matrix renormalization group (DMRG) calculations, and find good agreement in the extreme limits. We use these analytical results to interpret the DMRG calculations in the intermediate-coupling regime (defined by $W \sim U$), most applicable to conjugated polymers. We make the following conclusions. (1) In the weak-coupling limit the bound states are Mott-Wannier excitons, i.e., conduction-band electrons bound to valence-band holes. Singlet and triplet excitons whose relative wave functions are odd under a reflection of the relative coordinate are degenerate. Thus, the $2\,^{1}A_{g}^{+}$ and $1\,^{3}A_{g}^{-}$ states are degenerate in this limit. (2) In the strong-coupling limit the bound states are Mott-Hubbard excitons, i.e., particles in the upper Hubbard band bound to holes in the lower Hubbard band. These bound states occur in doublets of even and odd parity excitons. Triplet excitons are magnons bound to the singlet excitons, and hence are degenerate with their singlet counterparts. (3) In the intermediate-coupling regime Mott-Wannier excitons are the more appropriate description for large dimerization, while for the undimerized chain Mott-Hubbard excitons are the correct description. For dimerizations relevant to polyacetylene and polydiacetylene both Mott-Hubbard and Mott-Wannier excitons are present. (4) For all coupling strengths an infinite number of bound states exist for $1/r$ interactions for an infinite polymer. As a result of the discreteness of the lattice and the restrictions on the exciton wave functions in one dimension, the progression of states does not follow the Rydberg series. In practice, excitons whose particle-hole separation exceeds the length of the polymer can be considered unbound. (5) The DMRG calculated exciton excitation energies scale as the inverse of the chain length for short chains and the inverse of the square of the chain length for long chains. This fits the effective-particle-in-a-box model.

I. INTRODUCTION

Conjugated polymers have a particularly rich spectrum of excited states, including covalent (or spin-density-wave) states and ionic (or particle-hole states). The particle-hole states, and in particular bound particle-hole (or exciton) states are especially important for determining the linear and nonlinear optical properties of conjugated polymers. Thus, the problem of understanding the nature of the low-lying excitations in conjugated polymers remains a challenge for both experimentalists and theorists alike. In this paper we attempt to develop an understanding of the exciton states in conjugated polymers via a mixture of both theoretical and computational analysis.

The study of excitons in conjugated polymers has often been inspired by the treatment of excitons in bulk three-dimensional semiconductors.[1] In three-dimensional semiconductors the excitons arise from bound particle-hole excitations from the valence band to the conduction band. The excitons are usually weakly bound, with large particle-hole separations, and are well described by a hydrogenic model. Excitons in this limit are called Mott-Wannier excitons. This model of bound conduction band electrons and valence band holes can also be applied to conjugated polymers.[2–4] In conjugated polymers a one-dimensional hydrogenic model applies, although one difference between one and three dimensions is that in one dimension the first excited state (i.e., the

lowest bound state) is generally strongly bound, with a small particle-hole separation.[5] Such strongly bound excitons are akin to Frenkel excitons, which are delocalized intra-atomic excitations. However, for simplicity we prefer to label all excitons formed from bound states of conduction-band electrons and valence-band holes as Mott-Wannier excitons, recognizing that this term includes both small- and large-radius excitons. We call this limit the weak-coupling limit, as the starting point in the construction of the exciton basis is the noninteracting band limit.

More recently, an opposite, strong-coupling limit has been used to describe excitons in conjugated polymers.[6–8] In this limit a correlation gap separates the electron removal spectral weight (the lower Hubbard band) from the electron addition spectral weight (the upper Hubbard band). Now the bound particle-hole excitations are Mott-Hubbard excitons. That is, a particle, excited from the lower Hubbard band to the upper Hubbard band, is bound to the hole it leaves behind. In a real-space picture, this corresponds to two electrons in the same orbital bound to an empty orbital moving in a sea of singly occupied orbitals. A one-dimensional hydrogenic model also applies in this limit.[8]

In the context of π-conjugated polymers we can define the weak- and strong-coupling limits as follows. Suppose that t is the hybridization energy between π orbitals, and U is the electronic repulsion between two electrons in the same π orbital. Then the bandwidth $W = 4t$, and for weak cou-

pling $W \gg U$, while for strong coupling $W \ll U$.[9] Generally, conjugated polymers are in the intermediate regime, as $W \sim U$, so neither the weak nor strong-coupling limits apply. Since no theory has yet, to our knowledge, been developed for the intermediate regime, numerical calculations are the only means to theoretically study this limit.

In this paper we study excitons using the Pariser-Parr-Pople model (or extended Hubbard model) of π-conjugated polymers. This is a tight-binding model with long-range Coulomb interactions. We use the Ohno interaction, which is an interpolation between $1/r$ interactions for large r and an on-site Hubbard U. We solve the Pariser-Parr-Pople model using the density matrix renormalization group (DMRG) method.[10] We test the validity of the weak- and strong-coupling theories by comparing them to the DMRG calculations. Furthermore, we use the DMRG calculations to interpolate between these two limits in order to gain an understanding of the physically relevant intermediate regimes.

Our starting point is the Pariser-Parr-Pople model, defined as

$$H = -\sum_{i\sigma} t_i(c_{i\sigma}^\dagger c_{i+1\sigma} + c_{i+1\sigma}^\dagger c_{i\sigma})$$

$$+ U\sum_i n_{i\uparrow}n_{i\downarrow} + \sum_{ij} V_j n_i n_{i+j}. \qquad (1)$$

$c_{i\sigma}^\dagger$ creates an electron with spin σ in the π orbital on site i and $n_i = \sum_\sigma c_{i\sigma}^\dagger c_{i\sigma}$. V_j is the Coulomb repulsion, $V_j = U/\sqrt{1 + \beta r_j^2}$, where the bond lengths are in Å and $\beta = (U/14.397)^2$. The long and short bond lengths used in the evaluation of V_j are 1.45 and 1.36 Å, respectively, and the bond angle is 120°. The hybridization integral $t_i = t[1 + (-1)^i\delta]$, where δ is the bond dimerization parameter. We fix t at 2.5 eV, and vary both U and δ. In a realistic parameterization for π-conjugated systems, $U \sim 10$ eV. Linear polymers, such as polyacetylene and polydiacetylene, are therefore in the intermediate-coupling regime. For the phenyl-based systems, however, the electronic screening by the other electrons on the phenyl rings results in an effectively smaller local Coulomb interaction for the electrons in the bonding highest occupied molecular orbital (HOMO) and lowest unoccupied molecular orbital (LUMO). Modeling of phenyl-based systems with a two-band model suggests an effective U of between 3 and 4 eV, and a $\delta = 0.2$,[11] suggesting that the weak-coupling limit is more applicable for these systems.

In the next section we discuss the predictions and validity of the weak-coupling limit and compare them to the DMRG calculations. We show that the Mott-Wannier excitons are the so-called essential states that participate in the nonlinear optical spectroscopies.[12] We then discuss the strong-coupling limit in Sec. III, and show that here the Mott-Hubbard excitons form the essential states. In Sec. IV we discuss the DMRG calculations in the intermediate regime. Using our understanding of the weak- and strong-coupling limits we show that for certain values of the dimerization parameter (relevant to polyacetylene and polydiacteylene) there are two

families of essential states, with one family being the Mott-Wannier excitons and the other family being the Mott-Hubbard excitons. We conclude in Sec. V by comparing our predictions to a variety of conjugated polymers.

II. THE WEAK-COUPLING LIMIT

The weak-coupling limit takes as its starting point for the ground state the conventional semiconductor band picture of a filled valence band and an empty conduction band. A bound conduction-band electron and valence-band hole move through the lattice as an effective particle. In this section we derive the effective-particle model and compare it to the DMRG calculations.

A. The effective-particle model

In the weak-coupling limit it is convenient to regard the polymer chain as a linear chain of dimers, where each dimer represents a repeat unit. For polyacetylene the repeat unit is a double bond. For poly(para-phenylene) the repeat unit is a phenyl unit; however, an effective two-band model can be derived for the low-lying physics associated with the HOMO valence band and the LUMO conduction band.

Let $a_{k\sigma}^{v\dagger}$ and $a_{k\sigma}^{c\dagger}$ create electrons in Bloch states of the valence and conduction bands, respectively. In terms of the atomic orbital basis they are

$$a_{k\sigma}^{v\dagger} = \frac{1}{\sqrt{2}}[c_{1k\sigma}^\dagger \exp(i\phi_k/2) + c_{2k\sigma}^\dagger \exp(-i\phi_k/2)], \qquad (2)$$

and

$$a_{k\sigma}^{c\dagger} = \frac{1}{\sqrt{2}}[c_{1k\sigma}^\dagger \exp(i\phi_k/2) - c_{2k\sigma}^\dagger \exp(-i\phi_k/2)], \qquad (3)$$

where

$$c_{1k\sigma}^\dagger = \frac{1}{\sqrt{N_u}} \sum_l c_{2l-1\sigma}^\dagger \exp[i(2l-1)ka], \qquad (4)$$

$$c_{2k\sigma}^\dagger = \frac{1}{\sqrt{N_u}} \sum_l c_{2l\sigma}^\dagger \exp(i2lka), \qquad (5)$$

$\tan(\phi_k) = \delta\tan(ka)$, the sum is over unit cells, a is the lattice parameter, and N_u ($= N/2$) is the number of unit cells. $a_{k\sigma}^{v\dagger}$ and $a_{k\sigma}^{c\dagger}$ diagonalize Eq. (1) when $U = 0$, with energies of,

$$\epsilon_k^v = -2t[\cos^2(ka) + \delta^2\sin^2(ka)]^{1/2} \qquad (6)$$

for the valence band, and

$$\epsilon_k^c = 2t[\cos^2(ka) + \delta^2\sin^2(ka)]^{1/2} \qquad (7)$$

for the conduction band, where $k = 2\pi n/Na$ and $-N/4 \leq n \leq N/4$.

The corresponding Wannier molecular orbitals, localized on the lth repeat unit, are the Bloch transforms of Eqs. (2) and (3),

$$a_{l\sigma}^{v\dagger} = \frac{1}{\sqrt{N_u}} \sum_k a_{k\sigma}^{v\dagger} \exp(-i2lka) \qquad (8)$$

and

$$a_{l\sigma}^{c\dagger} = \frac{1}{\sqrt{N_u}} \sum_k a_{k\sigma}^{c\dagger} \exp(-i2lka). \qquad (9)$$

The ground state is constructed by filling the valence band,

$$|GS\rangle = \prod_k a_{k\uparrow}^{v\dagger} a_{k\downarrow}^{v\dagger} |0\rangle, \qquad (10)$$

or, equivalently in real space,

$$|GS\rangle = \prod_l a_{l\uparrow}^{v\dagger} a_{l\downarrow}^{v\dagger} |0\rangle. \qquad (11)$$

We may use either the k-space or real-space representations to construct an exciton basis. A basis state in real space is

$$|l+m/2, l-m/2\rangle = S_{lm}^{\dagger} |GS\rangle, \qquad (12)$$

where

$$S_{lm}^{\dagger} = \frac{1}{\sqrt{2}} (a_{l+m/2\uparrow}^{c\dagger} a_{l-m/2\uparrow}^{v} \pm a_{l+m/2\downarrow}^{c\dagger} a_{l-m/2\downarrow}^{v}). \qquad (13)$$

$S_{lm}^{\dagger}$ creates an electron in a conduction-band Wannier molecular orbital in the $(l+m/2)$th repeat unit, separated by m repeat units from a hole in a valence-band Wannier molecular orbital. The plus sign creates a singlet basis, while the minus sign creates a triplet basis. The general exciton eigenstate, $|\Psi^{MW}\rangle$, is then formed from a linear superposition of these basis states,

$$|\Psi^{MW}\rangle = \sum_{l,m} f(l,m) |l+m/2, l-m/2\rangle, \qquad (14)$$

where the coefficients, $f(l,m)$, are found from the appropriate exciton Hamiltonian, and MW refers to Mott-Wannier excitons.[13]

To proceed further it is necessary to recast the Pariser-Parr-Pople model in a molecular orbital basis. Furthermore, as a simplification, we assume that the Wannier molecular orbitals are localized on a particular dimer, i.e., we assume that

$$a_{l\sigma}^{v\dagger} \approx \tilde{a}_{l\sigma}^{v\dagger} \equiv \frac{1}{\sqrt{2}} (c_{2l-1\sigma}^{\dagger} + c_{2l\sigma}^{\dagger}) \qquad (15)$$

and

$$a_{l\sigma}^{c\dagger} \approx \tilde{a}_{l\sigma}^{c\dagger} \equiv \frac{1}{\sqrt{2}} (c_{2l-1\sigma}^{\dagger} - c_{2l\sigma}^{\dagger}). \qquad (16)$$

The inverse relations are thus

$$c_{2l-1\sigma}^{\dagger} \approx \frac{1}{\sqrt{2}} (a_{l\sigma}^{v\dagger} + a_{l\sigma}^{c\dagger}) \qquad (17)$$

and

$$c_{2l\sigma}^{\dagger} \approx \frac{1}{\sqrt{2}} (a_{l\sigma}^{v\dagger} - a_{l\sigma}^{c\dagger}). \qquad (18)$$

This approximation does not lead to any qualitative differences in the predictions, but does lead to the simplification of only having nearest-neighbor hopping terms in the next equation.[14]

Substituting Eqs. (17) and (18) into Eq. (1), the molecular orbital Hamiltonian,[11,15] is

$$H = -\sum_{l\gamma\sigma} \tilde{t}_{\gamma\gamma} (a_{l\sigma}^{\gamma\dagger} a_{l+1\sigma}^{\gamma} + a_{l+1\sigma}^{\gamma\dagger} a_{l\sigma}^{\gamma}) + \sum_{l\gamma} \epsilon_{\gamma} n_l^{\gamma}$$

$$+ \tilde{V}_0 \sum_{l\gamma} n_{l\uparrow}^{\gamma} n_{l\downarrow}^{\gamma} + \frac{\tilde{V}_0}{2} \sum_{l\gamma \neq \gamma'} n_l^{\gamma} n_l^{\gamma'} + \sum_{l \neq l' \gamma\gamma'} \tilde{V}_{l'} n_l^{\gamma} n_{l+l'}^{\gamma'}$$

$$- J \sum_{l\gamma \neq \gamma'} \left[\mathbf{S}_l^{\gamma} \cdot \mathbf{S}_l^{\gamma'} + \frac{1}{4} n_l^{\gamma} n_l^{\gamma'} \right], \qquad (19)$$

where $n_{l\sigma}^{\gamma} = a_{l\sigma}^{\gamma\dagger} a_{l\sigma}^{\gamma}$, $\mathbf{S}_l^{\gamma} = \Sigma_{\rho\rho'} a_{l\rho}^{\gamma\dagger} \sigma_{\rho\rho'} a_{l\rho'}^{\gamma}$, and σ are the Pauli spin matrices.[16] In terms of the atomic orbital parameters the molecular orbital parameters (denoted by a tilde) are

$$\tilde{t}_{vv} = -\tilde{t}_{cc} = t(1-\delta)/2,$$

$$\epsilon_v = -\epsilon_c = -t(1+\delta),$$

$$\tilde{V}_0 = (V_0 + V_1)/2, \qquad (20)$$

$$\tilde{V}_l = (V_{2l-1} + 2V_{2l} + V_{2l+1})/4,$$

$$J = (V_0 - V_1)/2.$$

The scalar product $\langle l+(m/2), l-(m/2)|H|\Psi^{MW}\rangle$ gives the following equation for $f(l,m)$:

$$-\tilde{t}\left[f\left(l+\frac{1}{2}, m-1\right) + f\left(l-\frac{1}{2}, m+1\right) + f\left(l-\frac{1}{2}, m-1\right) \right.$$

$$\left. + f\left(l+\frac{1}{2}, m+1\right) \right] + (2J\delta_{m0}\delta_M - \tilde{V}_l) f(l,m)$$

$$= (E - \tilde{V}_0 - \Delta + J) f(l,m), \qquad (21)$$

where $\Delta = \epsilon_c - \epsilon_v = 2t(1+\delta)$ is the HOMO-LUMO gap, and $\tilde{t} = t(1-\delta)/2$.

To derive an effective-particle model,[8,17] we introduce the center-of-mass coordinate, $R = (R_{l+m/2} + R_{l-m/2})/2 = ld$, and the relative coordinate, $r = R_{l+m/2} - R_{l-m/2} = md$, where d is the contour length between repeat units ($=2a$ for dimerised chains). For periodic boundary conditions we may assume that

$$f_n(l,m) = \frac{1}{\sqrt{N_u}} \exp(iKR) F_n(r), \qquad (22)$$

where K is the center-of-mass momentum: $-\pi/d \leq K \leq \pi/d$. For open boundary conditions we assume that

$$f_n(l,m) = \sqrt{\frac{2}{N_u+1}} \sin(\beta_j R) F_n(r), \qquad (23)$$

where β_j is the center of mass pseudomomentum: $\beta_j = j\pi/(N_u+1)d$, and $j = 1,2,\ldots,N_u$.

Substituting Eq. (22) into Eq. (21) the following difference equation for the relative wave function is obtained:

$$-2\tilde{t}\cos(Kd/2)[F_n(m-1) + F_n(m+1)]$$
$$+ (2J\delta_{m0}\delta_M - \tilde{V}_m)F_n(m) = (E - \tilde{V}_0 - \Delta + J)F_n(m), \qquad (24)$$

where $\delta_M = 1$ for singlet excitons, and $\delta_M = 0$ for triplet excitons.[18] $F_n(m)$ is the relative wave function for the electron-hole pair in the localized molecular orbitals m molecular repeat units apart. A similar equation for linear chains is obtained using Eq. (23), with β_j replacing K in Eq. (24).

Notice that two quantum numbers specify the exciton eigenstates, Eq. (22): the principle quantum number n and the (pseudo-) momentum, K (or β_j). For every n there are a family of excitons with different momenta. Odd and even values of n correspond to the relative wave function, $F_n(m)$, being even or odd under a reversal of the relative coordinate, respectively. We refer to even and odd parity excitons as excitons whose relative wave function is even or odd under a reversal of the relative coordinate. We do not mean that the overall parity of the eigenstate [Eq. (14)], determined by both the center-of-mass and relative wave functions, is even or odd. The number of nodes in the exciton wave function, $F_n(m)$, is $n-1$.

There are three important observations to be made about this effective-particle model. The first point is that since the exchange interaction is local (i.e., it is only nonzero when $m=0$), we immediately see that this term vanishes for odd parity excitons [i.e., $F_n(m) = -F_n(-m)$], as $F_n(0) = 0$. Now, since the parity of the exciton is determined by the particle-hole symmetry, and odd singlet and triplet excitons are determined by positive and negative particle-hole symmetries, respectively,[11] this theory predicts that $^1A_g^+$ and $^3A_g^-$ and the $^1B_u^+$ and $^3B_u^-$ excitons are degenerate.[2] (A derivation of the relation between particle-hole symmetry and particle-hole parity is given in Appendix A.)

The second observation is that when making the mapping from the atomic orbital Hamiltonian, to the molecular orbital Hamiltonian the distance between sites in the Coulomb interaction is replaced by the distance between molecular repeat units. For the polyacetylene structure the distance between double bonds is $\sqrt{3}a$. Thus, the Coulomb interaction has an *effective* dielectric constant of $\epsilon = \sqrt{3}$. An alternative and equivalent interpretation is that the effective mass is reduced by a factor of ϵ^2. Both interpretations lead to a reduction of the effective Rydberg by a factor of ϵ^2.

Finally, this model leads to unphysical predictions for large U, namely, that the lowest triplet has an energy below that of the ground state. This occurs when $J \gtrsim \Delta$, i.e., $U \sim 19.5$ eV for the Ohno potential.

We briefly discuss the continuum limit and the hydrogenic solutions of Eq. (24) in Appendix B. In the next section we analyze the general solutions to Eq. (24) and compare them to the DMRG calculations.

B. Comparison to the DMRG calculations

The DMRG calculations are performed on polymer chains with the polyacetylene geometry. Since these chains process C_2 symmetry the many-body eigenstates are either even, A_g, or odd, B_u. As discussed in Sec. II A, the singlet exciton wave function has even or odd parity when the particle-hole eigenvalue is odd or even. Conversely, the triplet exciton wave function has even or odd parity when the particle-hole eigenvalue is even or odd. As a consequence, we can express a $|{}^1B_u^-\rangle$ state as,

$$|{}^1B_u^-\rangle = \sum_{\text{odd } n} \sum_{\text{odd } j} \alpha_{nj} |\Psi_{nj}^{\text{MW}}\rangle + (\text{other contributions}), \qquad (25)$$

where $|\Psi_{nj}^{MW}\rangle$ is defined by Eqs. (14) and (23). Similarly, we can express the $|{}^1A_g^+\rangle$ state as

$$|{}^1A_g^+\rangle = \sum_{\text{even } n} \sum_{\text{odd } j} \alpha_{nj} |\Psi_{nj}^{\text{MW}}\rangle + (\text{other contributions}). \qquad (26)$$

Generally, the sums will be dominated by one component, except at anticrossings, as discussed shortly. The *other contributions* to the state vectors include, for example, covalent and holon-doublon terms.[19]

Figure 1 shows the binding energies of the singlet and triplet excitons as a function of U.[20] Since there is no exchange term in the binding energy of the triplets, their energies follow the predictions of the one-dimensional hydrogen-like model, namely, that the binding energy of the lowest exciton scales as U, while for large U the energies of the other excitons approaches the Rydberg series[5] (as discussed in Appendix B). In contrast, the exchange term affects the binding energies of the even parity singlet excitons. As a result of the functional form of the Ohno potential, which becomes steeper for small r as U increases, the exchange term increases with U. This leads to nonmonotonic behavior in the binding energies as a function of U.

We can compare these theoretical predictions to the DMRG calculations. We employ three ways of identifying the lowest pseudomomentum branch ($j=1$) of a given exciton family (n). First, these states have strong dipole moments connecting them. Second, there are jumps in the particle-hole separations, r_p, defined as,[11,21]
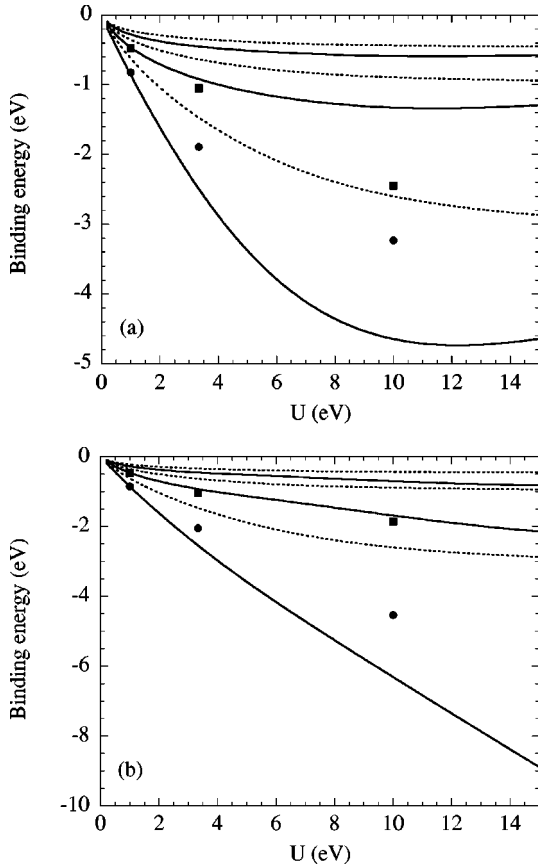
FIG. 1. Exciton binding energies in the weak-coupling limit. Even and odd parity excitons (with respect to the relative coordinate) are shown by solid and dashed curves, respectively. $t = 2.5$ eV and $\delta = 0.2$. The circles and squares are the DMRG calculations on 30-site chains for the $n=1$ and $n=2$ excitons, respectively. (a) Singlet and (b) triplet excitons.

$$r_p^2 = \langle m^2 \rangle_p = \frac{\sum_{lm} m^2 \langle p | S_{lm}^\dagger | \mathrm{GS} \rangle^2}{\sum_{lm} \langle p | S_{lm}^\dagger | \mathrm{GS} \rangle^2}. \qquad (27)$$

Finally, as shown in Fig. 3, energy plots against inverse chain length identify the different exciton families.

The DMRG calculations of the binding energies are shown for $U = 1, 10/3$, and 10 eV for 30 sites in Fig. 1. Except for $U = 1$ eV, the deviations between the weak-coupling theory and calculation are rather large. However, as Fig. 2 indicates, these deviations arise predominately from discrepancies in the predicted charge gap, rather than the exciton excitation energies. Figure 2 shows the two lowest singlet and triplet energies, and the charge gap. For $U = 1$ and $U = 10/3$ eV the agreement between the model and the DMRG calculations are good for the exciton energies. As predicted, the odd parity singlet and triplet excitons are degenerate. However, for $U = 10$ eV, the results are less good, particularly for the odd parity excitons. Further, the singlet and triplet are no longer degenerate, because the triplet exciton is evolving into a gapless spin density wave state.
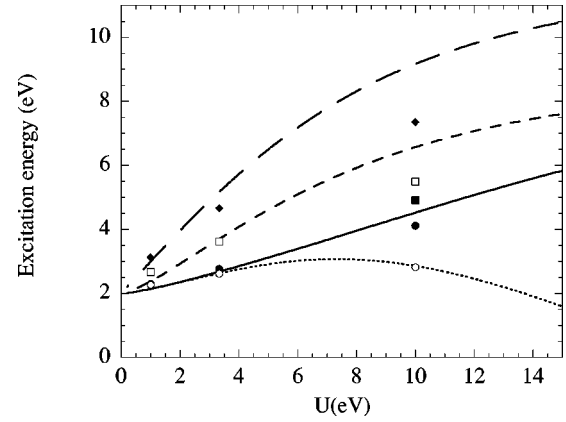
FIG. 2. The transition energies of the $n=1$ singlet (solid curve), $n=1$ triplet (dotted curve), $n=2$ singlet and triplet (short-dashed curve) excitons, and the charge gap (long-dashed curve) in the weak-coupling limit. $t = 2.5$ eV and $\delta = 0.2$. The circles and squares are the DMRG calculations on 30-site chains for the $n=1$ and $n=2$ excitons, respectively. The diamonds are the DMRG calculated charge gap. Singlet (solid symbols) and triplet (open symbols). The calculated $n=2$ singlet and triplet energies overlie each other at $U = 1$ and $10/3$ eV. The small discrepancies at $U = 1$ eV arise from finite-size effects.

There is a large disagreement between theory and calculation for the band gaps for large U. The origin of this disagreement is that the unbound particle-hole pair is strongly solvated by intrachain screening. The excitons are also solvated, but this solvation becomes less strong as the excitons become more strongly bound. This intrachain screening cannot simply be modeled by an effective dielectric constant, although this would reduce the exciton binding energies, it would not affect the band gap.

The evolution of the calculated exciton energies as function of chain length shows a number of interesting features. Fig 3(a) and 3(b) show the $^1B_u^-$ (odd n) and $^1A_g^+$ (even n) spectra, respectively. The different pseudomomentum (j) states for the same n, and anticrossings between states of different n are clearly seen. Figure 3(a) shows the $n=1$ and $n=3$ excitons converging to 2.6 eV and 3.9 eV, respectively, while Fig. 3(b) shows the $n=2$ and $n=4$ excitons converging to 3.5 eV and 4.1 eV, respectively. The band gap is also shown converging to 4.4 eV. Thus, for 102 sites, there are at least four families of bound excitons. Figures 3(c) and 3(d) show the energies of the three lowest pseudomomentum branches of the lowest $^1B_u^-$ ($n=1$) and $^1A_g^+$ ($n=2$) excitons (i.e., $j=1,3$, and 5) as a function of the square of the inverse chain length. The ratios of their slopes are 1:9:25, showing that the energies scale as $1/N^2$, indicating particle-in-a-box behavior.[8]

The particle-hole separations are shown in Fig. 4 at 102 sites. The jumps in the separation occur at $p=9$ and $p=8$ for the even and odd parity excitons, respectively, corresponding to the $j=1$ branches of the $n=3$ and $n=4$ excitons. Notice that, as predicted in Ref. 8 and Appendix B, the particle-hole separations decrease with increasing j for the same n. As a comparison to the DMRG calculations, we plot the exciton probability functions derived from the weak-coupling limit in Fig. 5.
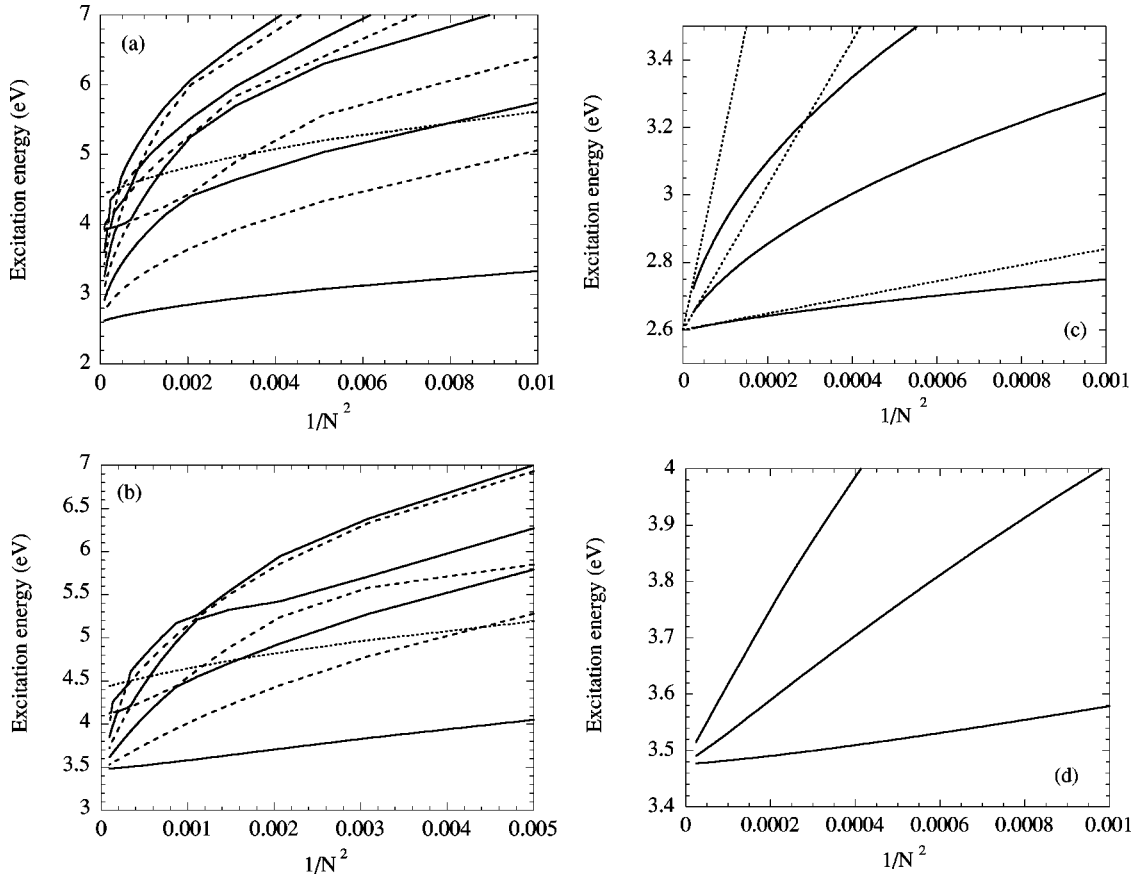
FIG. 3. The DMRG calculated singlet exciton transition energies as a function of square of the inverse chain length. $t = 2.5$ eV, $U = 10/3$ eV, and $\delta = 0.2$. All curves are for odd pseudomomentum quantum number, j. Solid and dashed curves are to illustrate the anticrossings. Also shown is the charge gap as the dotted curve. (a) $^1B_u^-$ states (odd n), showing the $n = 1$ exciton converge to 2.6 eV and the $n = 3$ exciton converge to 3.9 eV. (b) $^1A_g^+$ states (even n), showing the $n = 2$ exciton converge to 3.5 eV and the $n = 4$ exciton converge to 4.1 eV. (c) The first three $^1B_u^-$ states, showing straight line fits of relative gradients 1:9:25. (d) The first three $^1A_g^+$ states.

A comparison between the DMRG results and the weak coupling theory is shown in Table I. For the $n = 1$ and $n = 2$ excitons the agreement between the excitation energies is good, but, as discussed above, the binding energies do not agree well.

We conclude this section with a few remarks on the "essential" states responsible for the nonlinear optical susceptibilities. There are at most four states in a particular excitation path way in the sum-over-states calculation of $\chi^{(3)}$. Mazumdar and co-workers observed[12] that only a few excitation pathways (and hence states) contribute to this sum. The pathway must contain strong dipole moments to the ground state. In the weak coupling limit these are the $1\,^1A_g^+$, $1\,^1B_u^-$, $2\,^1A_g^+$, and $n\,^1B_u^-$ states, i.e., the ground state and the $n = 1, 2$ and 3 Mott-Wannier excitons.[22]

III. THE STRONG-COUPLING LIMIT

The strong-coupling limit for nearest-neighbor interactions was studied in Refs. 6 and 7, while an effective-particle model for general interactions was derived in Ref. 8. Excitons in this limit are quite different from their counterparts in the weak-coupling limit. In the weak-coupling limit excitons are particle-hole excitations from the valence to the conduction band. As we saw in Sec. II a real-space picture corresponds to a particle in a local antibonding molecular orbital bound to a hole in local bonding molecular orbital. Since an electron and hole can exist on the same dimer there are no restrictions on the symmetries of the relative wave function, and both singlet and triplet excitons exist. The strong-coupling limit starts from the approximation that the Coulomb interactions are so large that the undimerized band splits into a lower and upper Hubbard band. At half-filling the lower Hubbard band is full, corresponding to one electron per π orbital. Now an exciton is a particle in the upper Hubbard band bound to a hole in the lower Hubbard band, or an empty orbital bound to doubly occupied orbital on another site. These are Mott-Hubbard excitons. As shown in Ref. 7, this problem maps onto the problem of two bound spinless fermions (or hard-core bosons). The particle and hole cannot exist on the same site, so there is a local hard-core repulsion, and the relative wave function is zero for $r = 0$. In the continuum limit with a $1/r$ potential the bound states form a Rydberg series, with each energy level being composed of an even and odd pair of states.[8]

The general particle-hole eigenstate in this limit is of the form
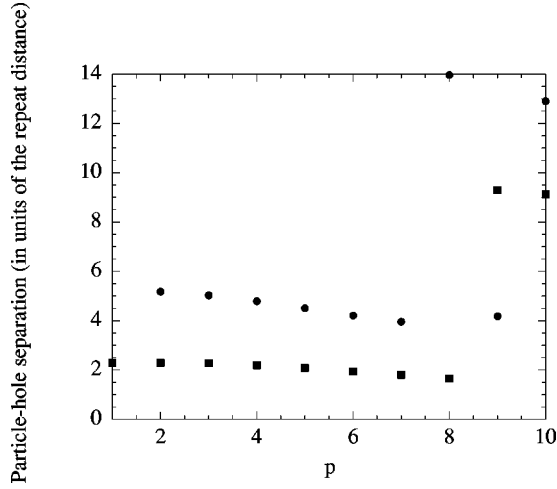
FIG. 4. The DMRG calculated root-mean-square particle-hole separations, r_p [Eq. (27)] in units of the molecular repeat distance, for 102 sites. $t = 2.5$ eV, $U = 10/3$ eV, and $\delta = 0.2$. $p\,^1B_u^-$ states (squares) and $p\,^1A_g^+$ states (circles). The molecular repeat distance is twice the lattice distance.

$$|\Psi^{MH}\rangle = \sum_{ii'} f_n(i,i')|i+i'/2, i-i'/2\rangle, \qquad (28)$$

where $|i+i'/2, i-i'/2\rangle = \Sigma_\sigma d^\dagger_{i+i'/2,\sigma} h^\dagger_{i-i'/2,\sigma}|GS\rangle$, and the MH refers to Mott-Hubbard excitons.

$$h^\dagger_{i\sigma} = c_{i\sigma}(1-n_{i\bar\sigma}) \qquad (29)$$

creates a holon (i.e., removes a particle with spin σ from the lower Hubbard band), while

$$d^\dagger_{i\sigma} = c^\dagger_{i\sigma} n_{i\bar\sigma} \qquad (30)$$

creates a doublon (i.e., creates a particle with spin σ in the upper Hubbard band).

Following the same procedure as in Sec. II, the relative wave function $F(i)$, Eq. (22), satisfies

$$-2t\cos(Ka/2)[F_n(i-1)+F_n(i+1)]-V_iF_n(i)$$
$$= (E-U)F_n(i), \qquad (31)$$
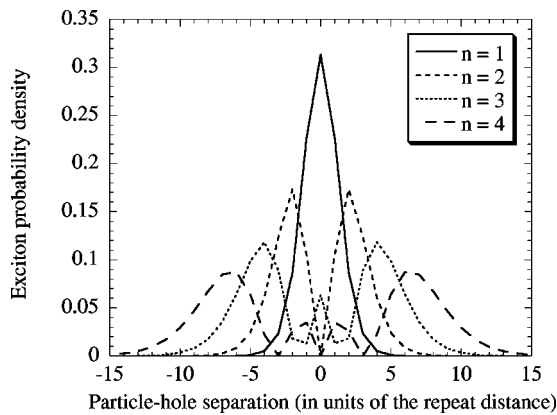
FIG. 5. The singlet exciton probability density, $F_n(m)^2$, in the weak-coupling limit. $t = 2.5$ eV, $U = 10/3$ eV, and $\delta = 0.2$.

TABLE I. The excitation energies and binding energies (in eV) for the first four $j = 1$ Mott-Wannier excitons of a 102-site chain. $\delta = 0.2$, $U = 10/3$ eV, and $t = 2.5$ eV.

State	DMRG calculation		Weak-coupling theory	
	Excitation energy	Binding energy	Excitation energy	Binding energy
$1\,^1B_u^-$ ($n=1$)	2.62	1.82	2.68	2.49
$2\,^1A_g^+$ ($n=2$)	3.49	0.95	3.70	1.47
$9\,^1B_u^-$ ($n=3$)	3.93	0.51	4.25	0.92
$8\,^1A_g^+$ ($n=4$)	4.13	0.31	4.54	0.63

where i is the distance between atomic orbitals. The hard-core repulsion, imposed by the condition $F_n(0) = 0$, implies that even and odd parity solutions are degenerate, because $F_n(i)$ can be matched by either $\pm F_n(-i)$ at the origin.

In analogy with Eqs. (25) and (26) we can express the exciton states as

$$|{}^1B_u^-\rangle = \sum_{\text{odd } n} \sum_{\text{odd } j} \beta_{nj}|\Psi^{MH}_{nj}\rangle + (\text{other contributions})$$
$$(32)$$

and

$$|{}^1A_g^+\rangle = \sum_{\text{even } n} \sum_{\text{odd } j} \beta_{nj}|\Psi^{MH}_{nj}\rangle + (\text{other contributions}),$$
$$(33)$$

where $|\Psi^{MH}_{nj}\rangle$ is defined in Eq. (28).

Since the unbound continuum starts at $U-4t$, we see that this model is unphysical for $U \lesssim 4t$, as then the bound states would have a negative excitation energy. So, although we can obtain binding energies, we cannot obtain physically realistic excitation energies in the intermediate-coupling regime. However, as we shall see in Sec. IV, this theory does provide qualitative insight to the behavior of the intermediate-coupling regime.

We check the theory against DMRG calculations. Figure 6 shows the binding energies as a function of U, with compari-
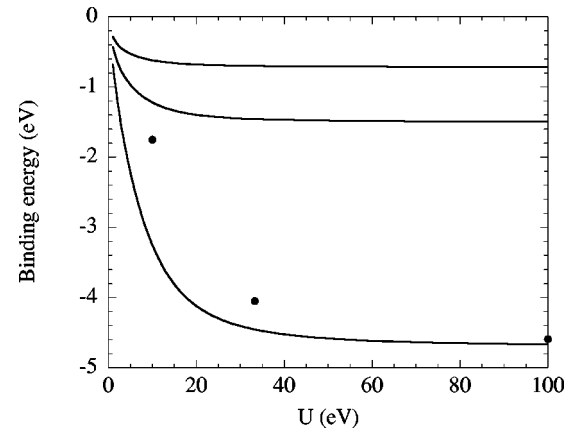
FIG. 6. The exciton binding energies in the strong-coupling limit. $t = 2.5$ eV and $\delta = 0$. The circles are the DMRG calculations for the $n = 1$ exciton on 30-site chains.

TABLE II. Excitation energies (in eV) of the key low-lying states for the undimerized 6-site chain. $U = 100$ eV and $t = 2.5$ eV.

State	Character	Excitation energy (eV)
$2\,^1A_g^+$	Pair of bound magnons	0.365
$1\,^1B_u^-$	$n=1$ Mott-Hubbard singlet exciton	86.375
$5\,^1A_g^+$	$n=2$ Mott-Hubbard singlet exciton	86.650
$1\,^3B_u^+$	Magnon	0.138
$1\,^3A_g^-$	Magnon bound to the $n=1$ Mott-Hubbard exciton	86.545
$8\,^3B_u^+$	Magnon bound to the $n=2$ Mott-Hubbard exciton	86.819

sons to DMRG calculations for $\delta = 0$. At large U the theory becomes exact, and also agrees very well with dimerized chains.

This strong-coupling exciton theory completely neglects the low-lying spin density wave excitations; nor does it describe the triplet excitons. In this limit the $1\,^3B_u^+$ state is a gapless spin-density wave, and not the $n=1$ Mott-Wannier triplet exciton, while the $2\,^1A_g^+$ state has evolved from the weak-coupling $n=2$ Mott-Wannier exciton to a pair of bound triplets.[23,24] This can be seen from the DMRG calculations for six sites, presented in Table II. The first odd parity singlet exciton is the $5\,^1A_g^+$ state, which is ca. $4t^2/(U-V_1)$ higher in energy than its associated even parity exciton, the $1\,^1B_u^-$ state. We interpret the $1\,^3A_g^-$ state as the $1\,^3B_u^+$ triplet bound to the $1\,^1B_u^-$ exciton, while the $8\,^3B_u^+$ state is the $1\,^3B_u^+$ triplet bound to the $5\,^1A_g^+$ exciton.

IV. THE INTERMEDIATE-COUPLING REGIME

As the strength of the Coulomb interactions are increased from the weak-coupling limit the character of the ground state and excitations changes. As discussed in Sec. III, a new class of excitations emerges, and these are the spin-density-wave (or covalent) states. The lowest lying triplet ($1\,^3B_u^+$) becomes a spin-density wave, and the $2\,^1A_g^+$ state evolves from the $n=2$ Mott-Wannier exciton to a pair of bound triplets. A higher-lying $^1A_g^+$ state evolves into the $n=2$ Mott-Hubbard exciton.

The intermediate-coupling regime is in the crossover between these regimes. In fact, the cross-over also occurs as a function of the dimerization δ. Consider the undimerized chain, with $\delta = 0$. As a result of the perfect nesting in one dimension there is always a correlation gap in the electronic spectrum of the half-filled chain for any nonzero Coulomb interaction. For the Hubbard model the correlation gap is $\sim \sqrt{Ut}\exp(-2\pi t/U)$ for $t \gg U$, while it is $U - 4t$ for $t \ll U$. We expect these predictions to remain qualitatively correct for long-range interactions. The correlation gap separates the lower and upper Hubbard bands. A particle-hole excitation across the correlation gap will result in a bound Mott-Hubbard exciton for any interaction strength, although for

weak interactions the exciton will be considerably more complicated than the holon-doublon exciton discussed in Sec. III. Alternatively, if the dimerization gap ($4t\delta$) is large compared to the correlation gap, we expect Mott-Wannier excitons to be the dominant low-energy ionic excitations.

We can see this behavior by studying the DMRG calculations. First, we consider $\delta = 0$. Figure 7(a) shows the four lowest essential states. The $1\,^1B_u^-$, $9\,^1A_g^+$, and $7\,^1B_u^-$ states are the $j=1$, $n=1$, 2, and 3 Mott-Hubbard excitons. The $2\,^1A_g^+$ state, with an energy lower than the $1\,^1B_u^-$ state, is predominately a bound triplet. The particle-hole separations in the holon-doublon channel, r_p, defined as[8]

$$ r_p^2 = \langle i'^2 \rangle_p = \frac{\sum_{ii'} i'^2 \langle p | \sum_\sigma d_{i\sigma}^\dagger h_{i+i'\sigma}^\dagger | GS \rangle^2}{\sum_{ii'} \langle p | \sum_\sigma d_{i\sigma}^\dagger h_{i+i'\sigma}^\dagger | GS \rangle^2}, \qquad (34) $$

are also shown.

Next we consider $\delta = 0.2$. Figure 7(b) shows that the four lowest essential states appear to fit the weak-coupling model, as they are the $1\,^1B_u^-$, $2\,^1A_g^+$, and $4\,^1B_u^-$ states. These are $j=1$, $n=1$, 2, and 3 Mott-Wannier excitons.

At $\delta = 0.1$ there are both Mott-Hubbard and Mott-Wannier excitons, forming two families of essential states. In general, the $^1B_u^-$ states are linear superpositions of Eqs. (25) and (32), while the $^1A_g^+$ states are linear superpositions of Eqs. (26) and (33), with one component predominating. As the bond dimerization decreases the spin-density-wave component of the $2\,^1A_g^+$ state increases.[25] Figure 7(c) shows the $1\,^1B_u^-$, $2\,^1A_g^+$, and $4\,^1B_u^-$ states, forming the Mott-Wannier family of excitons, while Fig. 7(d) shows the $1\,^1B_u^-$, $6\,^1A_g^+$, and $9\,^1B_u^-$ states, forming the Mott-Hubbard family of excitons. The progression of excitons in both families can also be identified by the jumps in the relevant particle-hole separation. These families are distinct in the sense that there are very small dipole moments between the $2\,^1A_g^+$ and $9\,^1B_u^-$ states and between the $6\,^1A_g^+$ and $4\,^1B_u^-$ states. However, since the $1\,^1B_u^-$ state has large dipole moments to both the $2\,^1A_g^+$ and $6\,^1A_g^+$ states, this state clearly has large amplitudes in both the $n=1$ Mott-Hubbard and $n=1$ Mott-Wannier families.

V. DISCUSSIONS AND CONCLUSIONS

In this paper we have analyzed effective-particle models for excitons in the weak- and strong-coupling limits, and compared them to DMRG calculations. There is good agreement between the effective-particle models and the computational results in these limits. These extreme limits have been used to understand the DMRG calculations in the intermediate-coupling regime. Our key conclusions are as follows.

(1) In the weak-coupling limit (where the single-particle gap is larger than the correlation gap) the bound states are Mott-Wannier excitons, i.e., conduction-band electrons bound to valence-band holes. Singlet and triplet excitons
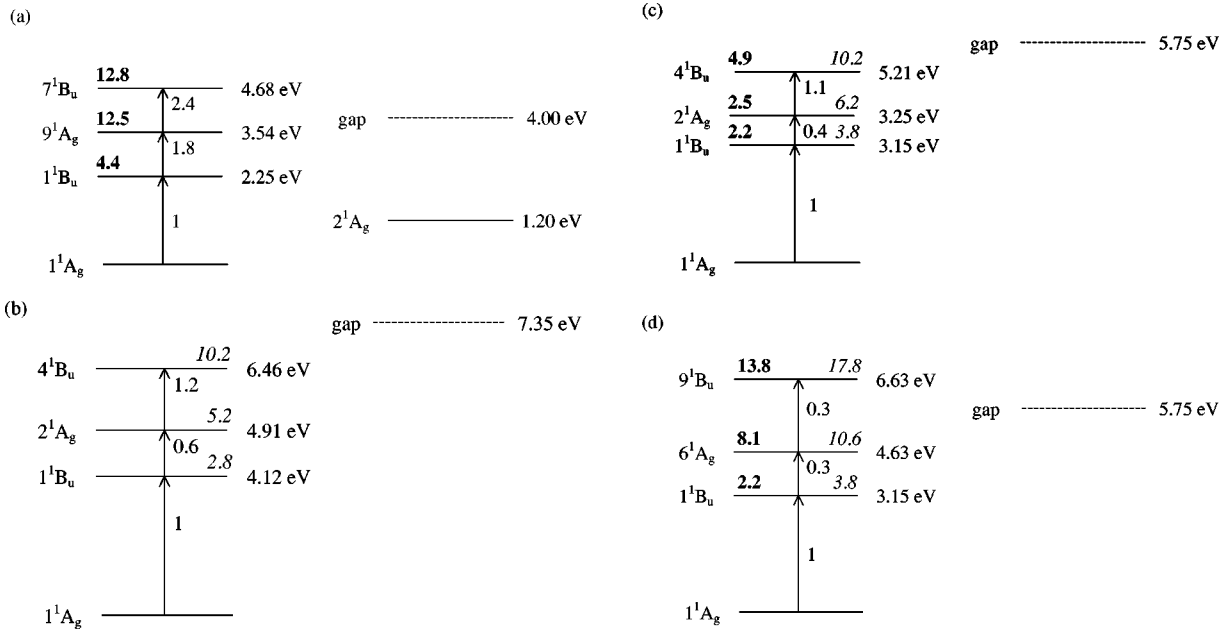
FIG. 7. The DMRG calculated essential states (defined as the four lowest states with the strongest inter-state dipole moments) for 30 site chains. The arrows show the dipole moments normalized to $1\,^1A_g^+ \to 1\,^1B_u^-$ dipole moment. The molecular-orbital and holon-doublon particle-hole separations (in units of the lattice spacing) are shown in italics using Eq. (27) and bold using Eq. (34), respectively. (a) $t = 2.5$ eV, $U = 10$ eV, and $\delta = 0$, showing the Mott-Hubbard series, (b) $t = 2.5$ eV, $U = 10$ eV, and $\delta = 0.2$, showing the Mott-Wannier series, (c) $t = 2.5$ eV, $U = 10$ eV and $\delta = 0.1$, showing the Mott-Wannier series, and (d) $t = 2.5$ eV, $U = 10$ eV and $\delta = 0.1$, showing the Mott-Hubbard series.

whose relative wave functions are odd under a reflection of the relative coordinate are degenerate. Thus, the $2\,^1A_g^+$ and $1\,^3A_g^-$ states are degenerate in this limit.

(2) In the strong-coupling limit (where the correlation gap is larger than the single particle gap) the bound states are Mott-Hubbard excitons, i.e., particles in the upper Hubbard band bound to holes in the lower Hubbard band. These bound states occur in doublets of even and odd parity excitons. Triplet excitons are magnons bound to the singlet excitons, and hence are degenerate with their singlet counterparts.

(3) In the intermediate-coupling regime Mott-Wannier excitons are the more appropriate description for large dimerization ($\delta = 0.2$), while for the undimerized chain Mott-Hubbard excitons are the correct description. For dimerizations relevant to polyacetylene and polydiacetylene (i.e., $\delta \sim 0.1$) both Mott-Hubbard and Mott-Wannier excitons are present.

(4) For all coupling strengths an infinite number of bound states exist for $1/r$ interactions for an infinite polymer. Generally, the effective-particle models overestimate binding energies, as they neglect intrachain screening. As a result of the discreteness of the lattice, and the restrictions on the exciton wave functions in one dimension, the progression of states does not follow the Rydberg series. In practice, excitons whose particle-hole separation exceeds the length of the polymer can be considered unbound. These predictions are in contrast to the those obtained from models with short-range interactions, which would predict one or more bound states in the weak-coupling limit, and zero or more bound states in the strong-coupling limit.[6,7]

(5) The DMRG calculated exciton excitation energies scale as the inverse of the chain length for short chains, and the inverse of the square of the chain length for long chains. This fits the effective-particle-in-a-box model.[8]

(6) The DMRG calculations show that the $n = 1$ exciton binding energy increases monotonically with increasing Coulomb interaction. At large coupling the binding energy agrees with the strong-coupling theory. We may therefore place a theoretical estimate on the binding energy of excitons in conjugated polymers as ca. 4.6 eV.

We can apply these exciton theories to actual conjugated polymers. Barford, Bursill, and co-workers have used the DMRG method to solve realistic parameterizations of the Pariser-Parr-Pople model for various systems.[26–29] Recent work[26] on poly(p-phenylene) puts the $1\,^1B_{1u}^-$ ($n = 1$) exciton at 3.7 eV, the $2\,^1A_g^+$ ($n = 2$) exciton at 5.1 eV and the $1\,^3A_g^-$ triplet close in energy to the $2\,^1A_g^-$ state, at 5.5 eV. This progression indicates a Mott-Wannier series of excitons. In contrast, polyacetylene and polydiacetylene have predominately Mott-Hubbard excitons. In polyacetylene the vertical energies of the $1\,^1B_{1u}^-$ and $2\,^1A_g^+$ states are virtually degenerate,[27] while for polydiacteylene the $2\,^1A_g^+$ state lies a few tenths of an eV higher than the $1\,^1B_{1u}^-$ state.[28] In both cases the $^1A_g^+$ state most strongly connected to the $1\,^1B_{1u}^-$ state is not the $2\,^1A_g^+$ state, but a higher $m\,^1A_g^+$ state, fitting the pattern of Mott-Hubbard excitons. Furthermore, in both cases the $2\,^1A_g^+$ state undergoes strong electron-lattice relaxation, and its relaxed energy lies below that of the relaxed $1\,^1B_{1u}^-$ state.[27,29] This places polyacetylene and polydiacetylene on the correlated side of the intermediate-coupling regime.

Our results apply to the vertical excitations of single polymer chains. Various additional intrinsic and extrinsic effects can significantly modify excited energies. Covalent states, such as highly correlated $1\,^3B_u^+$ and $2\,^1A_g^+$ states, undergo significant electron-lattice relaxation, and as already stated, this leads to a reversal of the $1\,^1B_{1u}^-$ and $2\,^1A_g^+$ energies in polyacetylene and polydiacetylene.

An important extrinsic effect is solvation by the environment, and again, this significantly alters the energy of excited states. States with larger binding energy are less solvated than those that are weakly bound. Current estimates are that the $n=1$ exciton solvates by ca. 0.3 eV, the $n=2$ exciton solvates by ca. 0.6 eV, and the band gap solvates by ca. 1.5 eV.[30] Thus, the experimentally reported exciton binding energies of ca. 0.5–1.0 eV, for polydiactelyene and PPV, etc., are much smaller than the bare single-chain values calculated here.

In conclusion, we have developed exciton theories for single chains with long-range interactions. It remains a challenge to predict the experimental signatures of these exciton states, especially when the additional intrinsic and extrinsic effects are included.

ACKNOWLEDGMENTS

APPENDIX A: PARTICLE-HOLE SYMMETRY AND PARTICLE-HOLE PARITY

In this appendix we prove that the relative parity of singlet particle-hole excitations is even or odd when the particle-hole symmetry is odd or even, respectively, and *vice versa* for triplet excitations. Using the definition that the particle-hole operator maps the atomic orbital creation operators as

$$c_{i\sigma}^\dagger \mapsto (-1)^i c_{i\bar\sigma}^-, \tag{A1}$$

it is easily shown, using Eqs. (8) and (9), that the creation operators for the conduction- and valence-band Wannier orbitals map as

$$a_{l\sigma}^{c\dagger} \mapsto -a_{l\bar\sigma}^v. \tag{A2}$$

Then, the singlet particle-hole basis state,

$$|l+m/2,l-m/2\rangle$$

$$=\frac{1}{\sqrt2}(a_{l+m/2\uparrow}^{c\dagger}a_{l-m/2\uparrow}^v+a_{l+m/2\downarrow}^{c\dagger}a_{l-m/2\downarrow}^v)|GS\rangle$$

$$\mapsto\frac{1}{\sqrt2}(a_{l+m/2\downarrow}^v a_{l-m/2\downarrow}^{c\dagger}+a_{l+m/2\uparrow}^v a_{l-m/2\uparrow}^{c\dagger})|GS\rangle$$

$$=-\frac{1}{\sqrt2}(a_{l-m/2\uparrow}^{c\dagger}a_{l+m/2\uparrow}^v+a_{l-m/2\downarrow}^{c\dagger}a_{l+m/2\downarrow}^v)|GS\rangle$$

$$=-|l-m/2,l+m/2\rangle \tag{A3}$$

under the particle-hole transformation. Thus, the particle-hole adapted-symmetry state

$$|l,m;\mp\rangle=\frac{1}{\sqrt2}(|l+m/2,l-m/2\rangle\pm|l-m/2,l+m/2\rangle) \tag{A4}$$

has a negative particle-hole symmetry eigenvalue for the even parity combination and a positive particle-hole symmetry eigenvalue for the odd parity combination.

The reverse relation holds for triplets, because the triplet particle-hole basis state

$$|l+m/2,l-m/2\rangle$$

$$=\frac{1}{\sqrt2}(a_{l+m/2\uparrow}^{c\dagger}a_{l-m/2\uparrow}^v-a_{l+m/2\downarrow}^{c\dagger}a_{l-m/2\downarrow}^v)|GS\rangle$$

$$\mapsto\frac{1}{\sqrt2}(a_{l+m/2\downarrow}^v a_{l-m/2\downarrow}^{c\dagger}-a_{l+m/2\uparrow}^v a_{l-m/2\uparrow}^{c\dagger})|GS\rangle$$

$$=+\frac{1}{\sqrt2}(a_{l-m/2\uparrow}^{c\dagger}a_{l+m/2\uparrow}^v-a_{l-m/2\downarrow}^{c\dagger}a_{l+m/2\downarrow}^v)|GS\rangle$$

$$=+|l-m/2,l+m/2\rangle, \tag{A5}$$

under the particle-hole transformation. Note that this relation between particle-hole symmetry and particle-hole parity holds for all exciton center-of-mass momenta, K, and not just $K=0$, as stated in Ref. 3.

APPENDIX B: "HYDROGENIC" SOLUTIONS TO THE EFFECTIVE-PARTICLE MODEL IN THE WEAK-COUPLING LIMIT

In this appendix we briefly examine the properties of the weak-coupling effective-particle model, Eq. (24), in the continuum limit. In making the connection to the continuum limit it is convenient to set $\tilde t=\hbar^2/2Md^2$, so $2\tilde t=\hbar^2/2\mu d^2$, where the reduced mass, $\mu=M/2$, and M is the effective mass. Then, scaling lengths by the effective Bohr radius, $a_0(K)=\hbar^2\cos(Kd/2)/\mu e^2$ and the energy by the effective Rydberg, $E_I(K)=\mu e^4/2\hbar^2\cos(Kd/2)$, we obtain

$$-\frac{1}{a'(K)^2}[F_n(m-1)+F_n(m+1)]-\frac{2F_n(m)}{a'(K)(1+m^2)^{1/2}}$$

$$=[E_n'(K)-\tilde V_0'-\Delta']F_n(m), \tag{B1}$$

where $a'(K)=d/a_0(K)$, $E_n'(K)=E_n/E_I(K)$, $\tilde V_0'=\tilde V_0/E_I(K)$, and $\Delta'=\Delta/E_I(K)$. We have used the Ohno function for the Coulomb interaction, which remains finite as $m\to0$, and we set $\tilde J=0$, as we are uninterested in details of the exchange splitting.[31]

In the continuum limit $[a'(K) \to 0]$ Eq. (B1) is identical (except for the regularization of the Coulomb term) to the effective one-dimensional equation for the radial part of the three-dimensional hydrogen atom wave function, $u(r) = r\psi(r)$, with zero angular momentum. This equation was studied in detail by Loudon.[5] The odd parity states have the same boundary conditions as $u(r)$, namely $u(0)=0$ and $u(r \to \infty) \to 0$. They are formed by matching $u(r)$ with $-u(-r)$ at the origin. Thus, for even n the binding energies are

$$E_n(K) = \frac{E_I(K)}{(n/2)^2} \qquad (B2)$$

and the corresponding wave functions are

$$F_n(r,K) = [Nr/a'(K)]\exp[-2r/na'(K)]L_{n/2}(4r/na'(K)), \qquad (B3)$$

where L_m is the mth-order Laguerre polynomial and N is a normalization constant.

The lowest even parity state is strongly bound, with a binding energy scaling as $2/a'(K)$, while the energies of the remaining even parity states are bounded by a higher and lower odd parity state. Notice that as a result of the K dependency of $E_I(K)$ the binding energies for a given n are larger for the higher center-of-mass momentum states. Similarly, the characteristic length, $a_0(K)$, decreases for higher-momentum states, resulting in a smaller particle-hole separation.
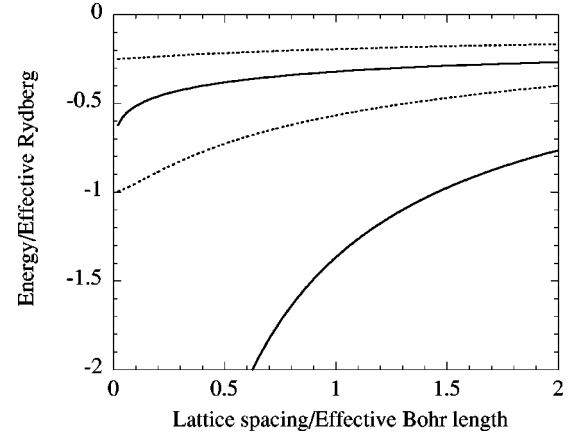
FIG. 8. The exciton binding energies in units of E_I in the weak-coupling limit for a regularized Coulomb potential versus a/a_I. Even parity, odd n states (solid curves) and odd parity, even n states (dashed curves).

For arbitrary $a'(K)$ it is necessary to solve Eq. (B1) numerically. Figure 8 shows the binding energy of the three lowest states at $K=0$ as a function of a'. As a' decreases the binding energies approach the Rydberg series, except for the energy of the first even parity state, which diverges. Typical values for conjugated polymers, with $t=2.5$ eV, are (i) $\delta=0.1$, which gives $E_I=3.90$ eV and $a'=1.31$, and (ii) $\delta=0.2$, which gives $E_I=4.40$ eV and $a'=1.48$. The resulting binding energies from Fig. 8 agree very well with those of Fig. 1(a).

*Email address: W.Barford@sheffield.ac.uk

[1] See, for example, R. S. Knox *Solid State Physics* (Academic, New York, 1963), Suppl. 5.

[2] A. Abe, J. Yu, W. P. Su, Phys. Rev. B **45**, 8264 (1992).

[3] D. Yaron and R. Silbey, Phys. Rev. B **45**, 11 655 (1992).

[4] D. Yaron, Phys. Rev. B **54**, 4609 (1996).

[5] R. Loudon, Am. J. Phys. **27**, 649 (1959).

[6] F. Gebhard, K. Bott, M. Scheidler, P. Thomas, and S. W. Koch, Philos. Mag. B **75**, 13 (1997); F. H. L. Essler, F. Gebhard, and J. Jeckelmann, Phys. Rev. B **64**, 12 5119 (2001).

[7] F. B. Gallagher and S. Mazumdar, Phys. Rev. B **56**, 15 025 (1997).

[8] W. Barford, Phys. Rev. B **65**, 205118 (2002).

[9] More correctly, we should define the weak-coupling limit when the noninteracting band gap is larger than the correlation gap, and *vice versa* for the strong-coupling limit. However, as no general expression exists for the correlation gap as a function of U/W we prefer our more qualitative definition.

[10] S. R. White, Phys. Rev. Lett. **69**, 2863 (1992); *Density Matrix Renormalization*, edited by I. Peschel, X. Wang, M. Kaulke, and K. Hallberg (Springer, Berlin 1999).

[11] W. Barford, R. J. Bursill, and M. Yu Lavrentiev, J. Phys.: Condens. Matter **10**, 6429 (1998).

[12] S. N. Dixit, D. Guo, and S. Mazumdar, Phys. Rev. B **43**, 6781 (1991); D. Guo, S. Mazumdar, S. N. Dixit, F. Kajzar, F. Jarka, Y. Kawabe, and N. Peyghambarian, *ibid.* **48**, 1433 (1993).

[13] A basis state in k space is $|k_h,k_e\rangle = S^{\dagger}_{k_e,k_h}|GS\rangle$, where $S^{\dagger}_{k_e,k_h}$

$= (1/\sqrt{2})(a^{c\dagger}_{k_e\uparrow}a^v_{k_h\uparrow} \pm a^{c\dagger}_{k_e\downarrow}a^v_{k_h\downarrow})$. k_e and k_h are the Bloch momenta of the electron and hole, respectively. The exciton eigenstate is $|\Psi^{MW}\rangle = \Sigma_{k_e,k_h} f_{k_e,k_h}|k_h,k_e\rangle$.

[14] The amplitude for the Wannier molecular orbital to overlap a neighboring dimer is very small. For $\delta=0.2$ this amplitude is 0.16, resulting in nearest-, next-nearest-, and next-next-nearest-neighbor hopping terms to be in the ratio of 1:0.17:0.06. Neglecting the longer range hopping terms means that the approximate single-particle bands differ from the exact single-particle bands, resulting in different effective masses and qualitatively different binding energies. Also, the two-electron parameters will be different. Thus, using the Wannier molecular orbitals rather than the local molecular orbitals will give a more accurate, but more complicated effective-particle theory; see Ref. 18.

[15] The general recipe for mapping between atomic orbital and molecular orbital Hamiltonians is given in R. J. Bursill, W. Barford, and H. Daly, Chem. Phys. **243**, 35 (1999).

[16] The molecular orbital Hamiltonian also contains terms that change the occupancy of the valence and conduction bands. However, as such terms do not connect basis states within the exciton sub-basis, they are neglected.

[17] D. C. Mattis, *The Theory of Magnetism* (Springer-Verlag, Berlin, 1981), p. 147.

[18] If next-nearest-neighbor hopping terms, $\tilde{t}_2$, are retained in Eq. (19), the difference equation becomes $-2\tilde{t}\cos(Kd/2)[F_n(m-1)+F_n(m+1)]-2\tilde{t}_2\cos(Kd)[F_n(m-2)+F_n(m+2)] + (2J\delta_{m0}\delta_M - \tilde{V}_m)F_n(m) = (E - \tilde{V}_0 - \Delta + J)F_n(m)$.

[19] Notice that odd n [i.e., even parity $F_n(m)$] and odd j (i.e., even center-of-mass wave function) implies $|^1B_u^-\rangle$, and even n [i.e., odd parity $F_n(m)$] and odd j implies $|^1A_g^+\rangle$, as the $\hat{C}_2$ operator reflects both the center-of-mass and relative coordinates, and hence exchanges the electron and hole.

[20] The binding energy is defined as the excitation energy relative to the charge gap, and the charge gap $= E(N+1) + E(N-1) - 2E(N)$. Although the charge gap is only truly meaningful for infinite chains, where the highest exciton energies become closely spaced and their particle-hole separations diverge, it is still a qualitatively useful concept for finite length chains, as it marks the energy above which a particle-hole excitation has more energy than an uncorrelated particle-hole pair.

[21] Notice that $\langle p|S_{lm}^\dagger|\mathrm{GS}\rangle = \Sigma_{nj}\alpha_{nj}$, and hence this is a measure of the exciton wave function.

[22] The anticrossings between a higher j of a lower n with the $j=1$ state of a higher n, shown in Fig. 3, can lead to spurious "essential states," as oscillator strength is transferred from the $j=1$ state of higher n to the higher j state of the lower n. These other essential states, arising from the accidental degeneracies, are quite different from the competing essential states seen in the intermediate-coupling regime, as discussed in Sec. IV.

[23] K. Schulten and M. Karpus, Chem. Phys. Lett. **14**, 299 (1972).

[24] P. Tavan and K. Schulten, Phys. Rev. B **36**, 4337 (1987).

[25] D. Mukhopadhyay, G. W. Hayden, and Z. G. Soos, Phys. Rev. B **51**, 9476 (1995).

[26] R. J. Bursill and W. Barford (unpublished).

[27] R. J. Bursill and W. Barford, Phys. Rev. Lett. **82**, 1514 (1999); W. Barford, R. J. Bursill, and M. Yu. Lavrentiev, Phys. Rev. B **63**, 195108 (2001).

[28] A. Race, W. Barford, and R. J. Bursill, Phys. Rev. B **64**, 035208 (2001).

[29] A. Race, W. Barford and R. J. Bursill (unpublished).

[30] E. Moore, B. Gherman, and D. Yaron, J. Chem. Phys. **106**, 4216 (1997); E. Moore and D. Yaron, *ibid.* **109**, 6147 (1998).

[31] In the continuum limit the exchange term diverges, leading to a diverging on-site repulsion for the singlet states. This reduces the binding energy of the even parity singlet states, so that each even parity state becomes degenerate with the higher-lying odd parity state. The onset of such behavior is seen in Fig. 1(a) for large U.